Cover Page

Universiteit Leiden

The handle http://hdl.handle.net/1887/22339 holds various files of this Leiden University dissertation.

Author: Szomoru, Daniel
Title: The extraordinary structural evolution of massive galaxies
Issue Date: 2013-11-21

MORPHOLOGICAL EVOLUTION OF GALAXIES FROM ULTRADEEP HST WFC3 IMAGING: THE HUBBLE SEQUENCE AT Z ∼ 2.

We use ultradeep HST WFC3/IR imaging of the HUDF to investigate the rest-frame optical morphologies of a mass-selected sample of galaxies at $z \sim 2$. We find a large variety of galaxy morphologies, ranging from large, blue, disk-like galaxies to compact, red, early-type galaxies. We derive rest-frame $u-g$ color profiles for these galaxies and show that most $z \sim 2$ galaxies in our sample have negative color gradients such that their cores are red. Although these color gradients may partly be caused by radial variations in dust content, they point to the existence of older stellar populations in the centers of $z \sim 2$ galaxies. This result is consistent with an ``inside-out'' scenario of galaxy growth. We find that the median color gradient is fairly constant with redshift: $(\Delta(u - g_{\mathrm{rest}})/\Delta(\log r))_{\mathrm{median}} = -0.47, -0.33$ and -0.46 for $z \sim 2$, $z \sim 1$ and $z = 0$, respectively. Using structural parameters derived from surface brightness profiles we confirm that at $z \sim 2$ galaxy morphology correlates well with specific star formation rate. At the same mass, star forming galaxies have larger effective radii, bluer rest-frame $u - g$ colors and lower Sérsic indices than quiescent galaxies. These correlations are very similar to those at lower redshift, suggesting that the relations that give rise to the Hubble sequence at $z = 0$ are already in place for massive galaxies at this early epoch.

Daniel Szomoru, Marijn Franx, Rychard J. Bouwens, Pieter G. van Dokkum, Ivo Labbé,
Garth D. Illingworth, Michele Trenti

3.1   INTRODUCTION

Since the description of the Hubble sequence (e.g., Hubble 1926; de Vaucouleurs 1959; Sandage & Tammann 1981) we have learned that position along the Hubble sequence correlates with parameters like color, stellar age, and gas fraction (e.g., Roberts & Haynes 1994). However, morphologies by themselves provide very limited information, as they are scale free and do not include physical parameters such as surface brightnesses, sizes, luminosities and masses. Using the Sloan Digital Sky Survey (SDSS, York et al. 2000), Kauffmann et al. (2003) showed that the main parameter driving galaxy properties is stellar mass. High-mass galaxies are generally red, have old stellar populations and low specific star formation rates (SSFRs), while low-mass galaxies are generally blue, have young stellar populations and high SSFRs.

A key question is what the structure was of the progenitors of low-redshift galaxies. Hubble Space Telescope studies out to redshift $z \sim 1$ indicate that the morphological variation is comparable to that at low redshift (e.g., Bell et al. 2004). More recent studies of $z > 2$ galaxies using the HST NICMOS camera have yielded varying results, largely due to different selection criteria. For example, Papovich et al. (2005) studied the rest-frame optical morphologies of a flux-limited sample of galaxies at $z \approx 2.3$ and found that they are generally irregular. Toft et al. (2005), on the other hand, investigated the rest-frame optical and UV morphologies of distant red galaxies (DRGs) in the Hubble Ultra Deep Field (HUDF), and found both galaxies with irregular morphologies and galaxies with smooth morphologies. Additionally, they showed that the rest-frame optical morphologies of these galaxies are much more regular and centrally concentrated than the rest-frame UV morphologies.

With the advent of the Wide Field Camera 3 (WFC3), with its vastly improved sensitivity and resolution compared to NICMOS, it has become possible to analyze the rest-frame optical structure of high-redshift galaxies with an unprecedented level of detail. Cameron et al. (2010) have used data from the first year of observations of the HUDF and the Early Release Science Field to classify the rest-frame UV and optical morphologies of galaxies up to $z \sim 3.5$. These authors confirm results by e.g. Kriek et al. (2009), who showed that massive galaxies at $z \approx 2.3$ can be separated into two distinct classes: blue star-forming galaxies with irregular morphologies on the one hand, and red quiescent galaxies with smoother morphologies on the other.

In this Letter, we extend the previous results using the full two-year ultradeep near-infrared imaging of the HUDF taken with the HST WFC3. These data are the deepest ever obtained in the near-infrared and make it possible to analyze the morphologies, colors and structure of galaxies to $z \sim 3$ in the rest-frame optical. Using the incredible sensitivity and angular resolution of the WFC3 images we analyze the rest-frame optical surface brightness profiles of a mass-selected sample of galaxies at $z \sim 2$. We use these profiles to derive structural parameters such as size and profile shape, and obtain rest-frame color profiles. We study the correlations between these parameters as a function of redshift in order to investigate the Hubble sequence at different epochs in the history of the Universe. Throughout the Letter, we assume a ΛCDM cosmology with $\Omega_m = 0.3$, $\Omega_\Lambda = 0.7$ and $H_0 = 70$ km s^{-1} Mpc^{-1}.
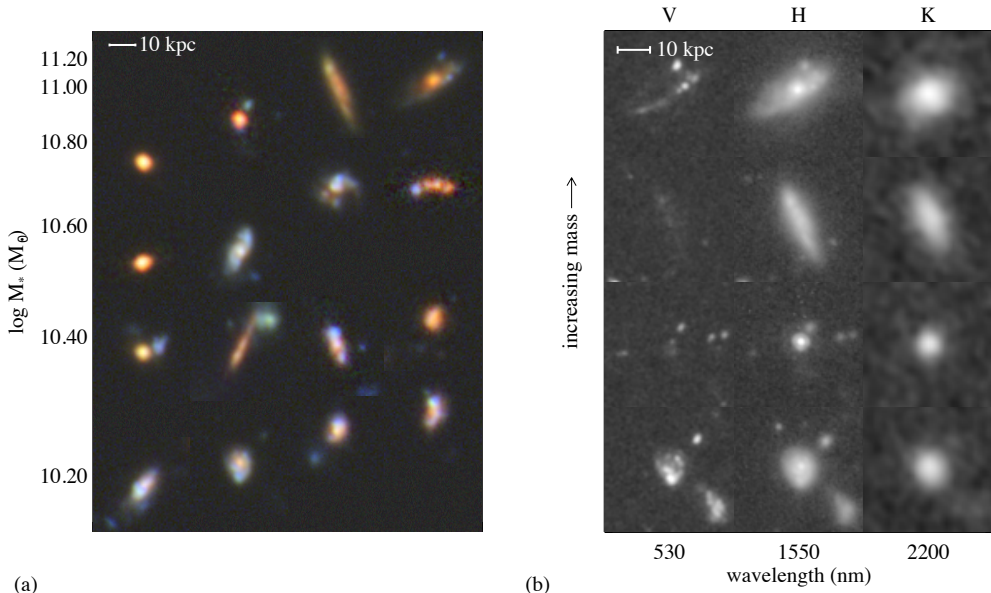
Figure 3.1: (*a*) Morphologies of $z \sim 2$ galaxies in the HUDF. The blue, green and red color channels are composed of PSF-matched HST/ACS i_{775}, HST/WFC3 Y_{105} and HST/WFC3 H_{160} images, respectively. Mass increases upwards. The galaxies exhibit a very large range in morphologies: from very compact, nearly unresolved spheroids with red colors, to large, extended disk-like galaxies with blue colors. Most of the galaxies have a well-defined center, which is usually redder than the outer parts of the galaxy. (*b*) Four massive galaxies at $z \sim 2$. From left to right, the galaxies are shown as observed in the HST/ACS V_{606} band, the HST/WFC3 H_{160} band, and the (ground-based) K_s band. The difference between the (PSF matched) V_{606} band and H_{160} band images is large: whereas the galaxies exhibit very regular morphologies and have well-defined centers in the H_{160} band, they are very clumpy and irregular in the V_{606} band, and in some cases are nearly undetected. These complex, wavelength-dependent morphologies suggest that $z \sim 2$ galaxies may be composed of multiple components with very different stellar ages.

3.2   MORPHOLOGIES AT Z $\sim$ 2

We use the full two-year data taken with WFC3/IR of the HUDF, obtained in 2009-2010 as part of the HUDF09 HST Treasury program (GO11563). It consists of 24 orbits of Y_{105} imaging, 34 orbits of J_{125} imaging, and 53 orbits of H_{160} imaging. These images were reduced using an adapted pipeline (Bouwens et al. 2010, Oesch et al. 2010). The FWHM of the PSF is ≈ 0.16 arcsec. The images are combined with very deep ACS images of the HUDF (Beckwith et al., 2006) to construct color images of the massive galaxies in the field.

We use the K_s-selected catalog of Wuyts et al. (2008) to select galaxies in the HUDF for which WFC3 imaging is available. This catalog combines observations of the Chandra Deep Field South ranging from ground-based U band data to Spitzer 24μm data, and includes spectroscopic redshifts where available, as well as photometric redshifts derived using EAZY (Brammer et al., 2008). Stellar masses were estimated from spectral energy distribu-

Table 3.1: Galaxy properties.

Source	ID[a]	mag_{app}^b (AB)	r_e^b (kpc)	n^b	$M_{stellar}^c$ ($M_\odot$)	$u - g_{rest}$	$\log \Sigma_{ave}$ ($M_\odot$ kpc^{-2})	z^c
HUDF09	3203	21.81	3.49	1.15	10.65	0.49	8.77	1.998
HUDF09	3239	23.11	0.32	2.06	10.51	1.18	10.72	1.980
HUDF09	3242	22.10	0.44	3.21	10.76	1.18	10.67	1.910
HUDF09	3254	23.31	1.96	1.31	10.25	0.85	8.87	1.887*
HUDF09	3391	23.28	2.13	0.44	10.37	-0.04	8.92	1.919*
HUDF09	3421	23.79	2.12	0.90	10.59	0.19	9.14	2.457*
HUDF09	3463	22.47	1.80	1.20	10.09	0.59	8.78	1.659*
HUDF09	3486	22.43	2.78	0.65	10.22	0.88	8.53	1.628*
HUDF09	3595	22.39	3.67	0.41	10.98	0.87	9.06	1.853*
HUDF09	3653	23.85	1.94	0.95	10.27	1.24	8.90	1.776*
HUDF09	3721	22.02	3.00	1.16	10.54	0.63	8.79	1.843
HUDF09	3757	23.10	1.25	5.04	10.28	1.20	9.29	1.674*
HUDF09	3799	24.59	2.93	1.50	10.62	0.87	8.89	2.492*
HUDF09	6161	21.58	6.70	3.51	11.08	1.22	8.63	1.552
HUDF09	6225	23.26	2.58	0.56	10.33	0.72	8.71	2.401*
HUDF09	6237	23.51	< 0.10	> 10.00	10.72	1.30	14.40	1.965*
...	...	...	...	...	...	...	...	...

This is a sample of the full table, shown for illustrative purposes.

[a] IDs correspond to NYU-VAGC IDs (Blanton et al., 2005) for the SDSS galaxies, and FIREWORKS IDs (Wuyts et al., 2008) for the HUDF galaxies

[b] Derived from the SDSS g band imaging for the SDSS galaxies, and from the HST/WFC3 H_{160} band imaging for the HUDF09 galaxies

[c] Obtained from the Guo et al. (2009) catalog for the SDSS galaxies, and the Wuyts et al. (2008) catalog for the HUDF galaxies. Masses are corrected to account for the difference between the catalog magnitude and our measured magnitude.

* No spectroscopic redshifts are available for these galaxies; photometric redshifts are listed instead

tion fits to the full photometric data set (Förster Schreiber et al., in preparation), assuming a Kroupa IMF and the stellar population models of Bruzual & Charlot (2003). To study the morphological variation at $z \sim 2$, we select the 16 most massive galaxies with $1.5 < z < 2.5$. These galaxies have stellar masses between 1.2×10^{10} M$_\odot$ and 1.3×10^{11} M$_\odot$. Color images of these galaxies are shown in Figure 3.1a. A summary of their properties is given in Table 3.1.

From Figure 3.1a it is apparent that galaxies at $z \sim 2$ show a large variation in morphology, size and color. One can distinguish red, smooth, compact galaxies; blue galaxies with disk-like structures, some even with apparent spiral arms; and other star forming galaxies which appear more irregular. Most of the galaxies have a well-defined, red center. This is further illustrated in Figure 3.1b, where galaxy morphology is shown as a function of wavelength. Four massive galaxies are shown in the observed HST/ACS V_{606} band (Beckwith et al., 2006), HST/WFC3 H_{160} band and K_s band (based on ground-based imaging by Labbé et al., in preparation). The morphology of the sources differs strongly as a function of wavelength. The rest-frame UV morphology is more clumpy and extended than the rest-frame

optical morphology. In addition, the rest-frame optical images show well-defined centers for all sources, whereas these are often lacking in the rest-frame UV images. This confirms that the mass distribution of $z \sim 2$ galaxies is smoother and more centrally concentrated than would be concluded from rest-frame UV imaging (see e.g., Labbé et al. 2003b; Toft et al. 2005).

3.3 COLOR GRADIENTS AT Z $\sim$ 2

In order to quantify the morphological properties of $z \sim 2$ galaxies we measure their surface brightness profiles. In contrast to conventional model-fitting techniques where a simple model is used to approximate the intrinsic surface brightness profile (e.g., using the GALFIT package of Peng et al. 2002), we measure the actual profile using the approach of Szomoru et al. (2010). The intrinsic profile is derived by fitting a Sérsic model profile convolved with the PSF to the observed flux, and then adding the residuals from this fit to the unconvolved model profile. Effectively, the model profile is used to deconvolve the majority of the observed flux, after which this deconvolved profile is combined with the residuals to account for deviations from the assumed model. Szomoru et al. (2010) have shown that it is thus possible to accurately measure the true intrinsic profiles out to large radii and very low surface brightness, even in cases where galaxies comprise a bright compact bulge and a faint extended disk.

In addition to the $z \sim 2$ galaxies we measure the profiles of galaxies at $z \sim 1$ and $z = 0$. The $z \sim 1$ sample is taken from the same dataset as the $z \sim 2$ sample, whereas the $z = 0$ galaxies are taken from the Guo et al. (2009) SDSS catalog of central galaxies. The galaxies are selected to lie in the same mass interval as the $z \sim 2$ sample: $1.2 \times 10^{10} M_\odot < M_{stellar} < 1.3 \times 10^{11} M_\odot$. The SDSS redshifts are required to be $z = 0.03 \pm 0.015$ and the $z \sim 1$ galaxies have $0.5 < z < 1.5$. This results in a sample of 27 galaxies at $z \sim 1$ and 84 galaxies at $z = 0$. Stellar masses and SSFRs for the SDSS sample are obtained from the MPA/JHU datarelease[1] (see Brinchmann et al. 2004; Salim et al. 2007 for details). A summary of the properties of the $z \sim 1$ and $z = 0$ galaxies is given in Table 3.1.

In Figure 3.2 we show surface density profiles, $u - g_{rest}$ color profiles, and $u - g_{rest}$ color gradients for galaxies in all three redshift bins. The surface density profiles are obtained by multiplying the surface brightness profiles in the H_{160} band (g band for the SDSS galaxies) with the galaxies' average $M_{stellar}/L$ ratios in that band (where $M_{stellar}$ is the total mass from the Wuyts et al. 2008 catalog (MPA/JHU catalog for the SDSS galaxies) and L is derived from the surface brightness profiles). This approach ignores gradients in the $M_{stellar}/L$ ratios and is therefore not exact; however, it allows for a more quantitative comparison between galaxies at different redshifts and with different colors. The color gradients are derived from fits to the $u - g$ profiles between the half-width at half-maximum
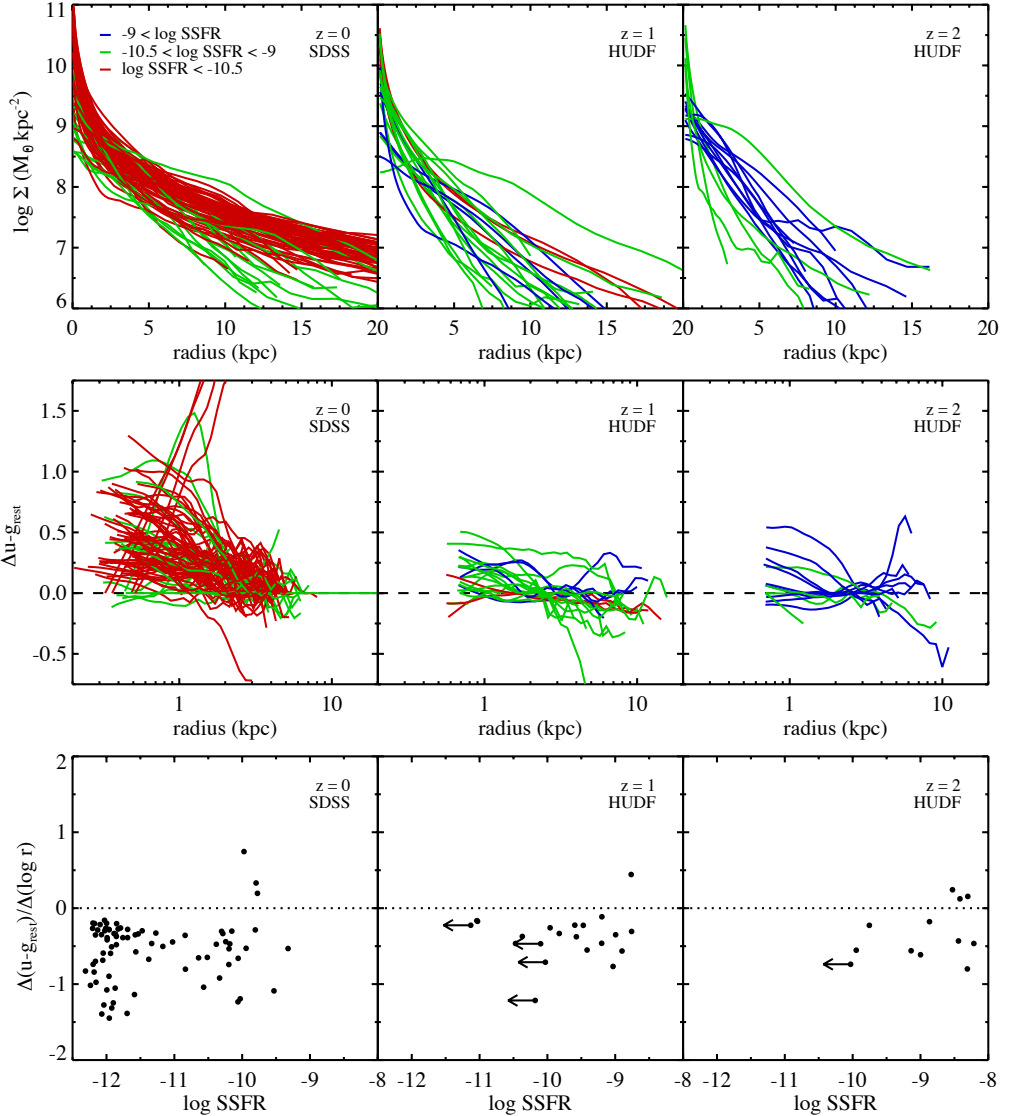
---

[1]http://www.mpa-garching.mpg.de/SDSS/

Figure 3.2: *Top panels:* surface density profiles of galaxies at $z = 0$, $z \sim 1$ and $z \sim 2$, color-coded according to specific star formation rate. The profiles are plotted up to the radius where uncertainties in the sky determination become significant. Surface density has been calculated from the average M/L_H (M/L_r for the SDSS galaxies) of the galaxy multiplied by the observed H_{160} (r_{625}) band surface brightness profile, ignoring gradients in the mass-to-light ratio. It is clear that a large diversity of profiles exists, with some close to exponential profiles and others close to $r^{1/4}$ profiles. This diversity extends to $z \sim 2$. *Middle panels:* $u - g_{rest}$ color profiles of the same galaxies. The profiles are normalized so that $\Delta u - g_{rest} = 0$ at $r = r_e$. The color profiles are plotted from the PSF HWHM (~ 0.6 arcsec for the SDSS galaxies, ~ 0.08 arcsec for the HUDF galaxies) to the radius where the errors in the flux measurement reach 20%. The color profiles show an overall trend of redder colors at smaller radii, in all redshift intervals. *Bottom panels:* $u - g_{rest}$ color gradients. Arrows indicate upper limits. Most $z \sim 2$ galaxies have negative color gradients. Color gradients do not seem to evolve very strongly between $z \sim 2$ and $z \sim 0$, for galaxies in the mass range considered here.

(HWHM) of the PSF (~ 0.6 arcsec for the SDSS galaxies, ~ 0.08 arcsec for the HUDF galaxies) and the radius where the errors in the flux measurement reach 20%.

The majority of $z \sim 2$ galaxies in our sample have negative color gradients, which do not vary strongly with redshift: $(\Delta(u - g_{\rm rest})/\Delta(\log r))_{\rm median} = -0.47^{+0.20}_{-0.56}, -0.33^{+0.19}_{-0.23}$ and $-0.46^{+0.58}_{-0.28}$ for $z \sim 2$, $z \sim 1$ and $z = 0$, respectively (where the errors give the 1-σ interval around the median). Thus, galaxy color gradients seem to be remarkably constant with redshift, both for quiescent and star-forming galaxies. It should be noted that this is not a comparison of low-redshift galaxies to their high-redshift progenitors; the $z \sim 2$ galaxies are expected to evolve into more massive galaxies at low redshift, due to mergers and accretion. Since we use mass-limited samples, the $z \sim 2$ galaxies we consider may fall outside of our mass-limits at low redshift. Selection by number density is better suited to trace the same population of galaxies across cosmic time (see, e.g., van Dokkum et al. 2010).

3.4 THE HUBBLE SEQUENCE FROM Z $\sim$ 2 TO Z = 0

Finally, we study the relations between structure, color and SSFR as a function of redshift in Figure 3.3. In the top row we show Sérsic index against SSFR for the $z = 0$, $z \sim 1$ and $z \sim 2$ samples. In the bottom row we show Sérsic index against rest-frame $u - g$ color for the same galaxies. The Sérsic indices are derived from fits to the residual-corrected H_{160}-band (g-band for the $z = 0$ galaxies) surface brightness profiles. There is a clear relation between these parameters at all redshifts: star-forming galaxies have ``diskier'' (lower n) profiles and bluer colors than quiescent galaxies. There is a large variation in the SSFRs, colors and Sérsic indices of $z \sim 2$ galaxies, and the spread in these parameters is of roughly the same order of magnitude in all redshift bins. The relation shows systematic evolution: the median SSFR increases with increasing redshift and the median color and Sérsic index decrease, from log SSFR $= -11.85^{+1.67}_{-0.22}$ yr^{-1} at $z = 0$ to log SSFR $= -8.87^{+0.50}_{-0.58}$ yr^{-1} at $z \sim 2$, from $u - g_{rest} = 1.62^{+0.38}_{-0.44}$ to $u - g_{rest} = 0.87^{+0.34}_{-0.33}$, and from $n = 4.25^{+1.71}_{-2.79}$ to $n = 1.20^{+2.16}_{-0.64}$ (where the errors give the 1-σ interval around the median). These results are qualitatively consistent with the trends derived in e.g., Franx et al. (2008).

The relations between structure, color and SSFR are further illustrated in Figure 3.4, which shows rest-frame $u - g$ color images of a selection of galaxies at $z = 0$, $z \sim 1$ and $z \sim 2$, as a function of SSFR. From each redshift bin we select seven galaxies, evenly spaced in log SSFR. This figure very clearly illustrates the morphological variety present at $z \sim 2$. Additionally, it confirms the relations shown in Figure 3.3: star-forming galaxies are blue and extended, while quiescent galaxies are red and relatively compact. Thus we find that the variation in galaxy structure at $z \sim 2$ is as large as at $z = 0$. Furthermore, the systematic relationships between different structural parameters are very similar between $z = 0$ and $z \sim 2$. This, in addition to the lack of evolution in the $u - g_{rest}$ color gradients shown in Figure 3.2, suggests that the underlying mechanisms that give rise to the Hubble sequence at $z = 0$ may already be in place at $z \sim 2$.
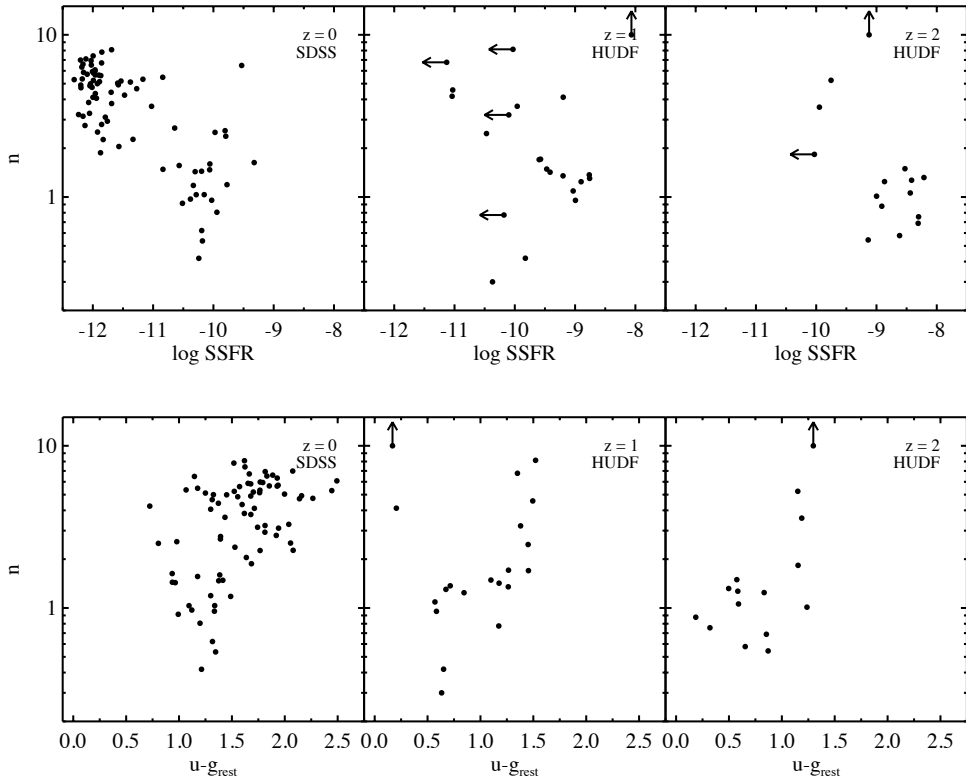
Figure 3.3: Sérsic index n plotted against SSFR (*top row*) and $u - g_{rest}$ color (*bottom row*) for galaxies with $1.2 \times 10^{10} M_\odot < M_{stellar} < 1.3 \times 10^{11} M_\odot$, at $z = 0$, $z \sim 1$ and $z \sim 2$. Arrows indicate upper or lower limits. Profile shape and SSFR are anticorrelated in all three wavelength bins, whereas profile shape and color show a positive correlation. The relations between these morphological parameters are similar in all three redshift bins, although on average galaxies are bluer and have higher SSFRs and lower Sérsic indices at high redshift. The similarity of the relations at $z = 0$ and $z \sim 2$ suggests that the Hubble sequence was already in place for massive galaxies at $z \sim 2$.

3.5 DISCUSSION

We have shown that the morphologies of massive $z \sim 2$ galaxies in the HUDF are complex and varied: from compact, apparently early-type galaxies to large star forming systems superficially similar to nearby spirals. Many of these galaxies seem to be composed of multiple components with large differences in stellar age. We conclude that the variety in morphologies which is observed at $z = 0$ also exists in galaxies at $z \sim 2$. This is confirmed by an analysis of the surface density profiles, which reveals a large range in profile shapes. The profiles of the large star forming systems are close to exponential, whereas the profiles of the quiescent systems are more concentrated. The correlations between morphology and SSFR are similar at all redshifts between $z = 0$ and $z \sim 2$.
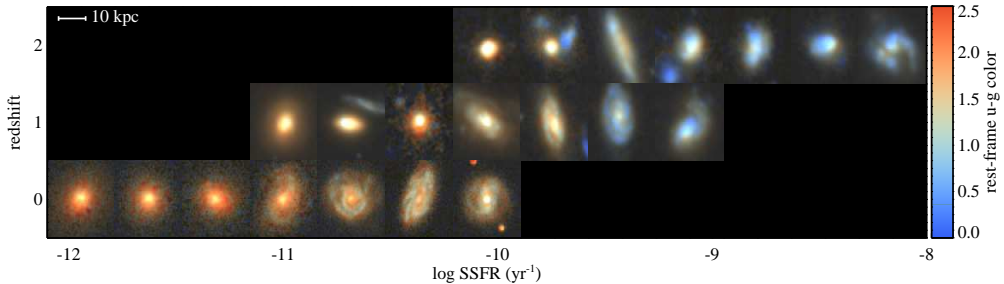
Figure 3.4: Galaxy morphologies from $z \sim 2$ to $z = 0$, as a function of SSFR. The colors of the galaxies have been obtained by scaling their rest-frame $u - g$ colors to the image's RGB space, as indicated by the color bar. The range in galaxy structure at $z \sim 2$ is very great, and is accompanied by a large range in galaxy colors. There is considerable evolution towards redder colors and lower SSFRs from $z \sim 2$ to $z = 0$. However, signs of a Hubble sequence (i.e., high-SSFR galaxies are ``diskier'', more extended and bluer than low-SSFR galaxies) appear to exist at $z \sim 2$.

This does not mean that morphologies and profiles are static: galaxies evolve quite strongly between $z = 2$ and $z = 0$. Quiescent galaxies are much more compact at high redshift, and cannot evolve passively into low-redshift quiescent galaxies (e.g., Daddi et al. 2005; Trujillo et al. 2006; Toft et al. 2007; van Dokkum et al. 2008). A similar size evolution is required for the star forming galaxies (e.g., Williams et al. 2010). We note that due to the evolution in the mass function of galaxies the $z \sim 2$ galaxies considered here will almost certainly not evolve into the low-redshift galaxies in this paper. It would be very informative to examine the morphologies of number density-limited galaxy samples over this redshift range, in order to investigate the evolution of the same galaxy population over time (e.g., van Dokkum et al. 2010).

Additionally, we have derived $u - g_{rest}$ color gradients of our galaxy sample, and have shown that massive $z \sim 2$ galaxies have negative color gradients that are comparable to those of low-redshift galaxies in the same mass range. These color gradients may partly be caused by radial variations in dust extinction, but radial changes in stellar populations likely play a large role (e.g., Abraham et al. 1999). This supports a galaxy growth scenario where small galaxies formed at high redshift grow by accreting material onto their outer regions. However, we lack the necessary information to rule out other possibilities; for example, if the gradients are caused by dust this might be an indication that these galaxies formed very quickly in a short burst.

The results seem to contrast with earlier analyses of galaxies at $z \sim 2$ in the HDFN (e.g., Dickinson 2000, Papovich et al. 2005). These authors concluded that all galaxies at this redshift are irregular and compact, with little difference between the rest-frame UV and optical. Field-to-field variations may play a role; as shown in Labbé et al. (2003a) the HDFN contains very few massive high-redshift galaxies. Indeed, the galaxies studied by these authors have lower masses ($M_{\rm stellar} \lesssim 3 \times 10^{10} M_\odot$) than the galaxies we consider,

which could result in the difference with the study presented here. Additionally, We note that recent kinematical studies of massive $z \sim 2$ galaxies also indicate that many contain gas with ordered motion (e.g., Genzel et al. 2008, Förster Schreiber et al. 2009, Tacconi et al. 2010). The results presented in this Letter are fully consistent with those.

Our results raise the question at what redshift the first ``ordered'' galaxies appeared, with structures similar to the Hubble sequence. There are indications that at redshifts beyond 3 such galaxies may be much harder to find. Typical high-redshift Lyman break galaxies are very clumpy and irregular (e.g., Lowenthal et al. 1997), and differ significantly in appearance from regular spiral galaxies. Furthermore, the population of massive galaxies that are faint in the UV may be very small at redshifts beyond 3 (e.g., Brammer & van Dokkum 2007), at least in the mass regime that is considered in this paper (e.g., Marchesini et al. 2010). With current observational capabilities we are severely limited in studying the rest-frame optical properties of galaxies at redshifts beyond $z \sim 3.5$, due to rest-frame optical emission moving redward of the observers' K band. With improved capabilities it may become possible to study the red massive galaxy population at these redshifts. Several candidates have been found at $z > 5$ with significant Balmer discontinuities (Eyles et al. 2005; Mobasher et al. 2005; Wiklind et al. 2008; Richard et al. 2011), and many more are speculated to exist. These galaxies could very well be the centers of multi-component galaxies at redshifts between $z = 3$ and $z = 5$.

REFERENCES

Abraham, R. G., Ellis, R. S., Fabian, A. C., Tanvir, N. R., & Glazebrook, K. 1999, MNRAS, 303, 641

Beckwith, S. V. W., et al. 2006, AJ, 132, 1729

Bell, E. F., et al. 2004, ApJ, 600, L11

Blanton, M. R., et al. 2005, AJ, 129, 2562

Bond, N. A., Gawiser, E., & Koekemoer, A. M. 2010, arXiv:1010.1525

Bouwens, R. J., et al. 2010, ApJ, 709, L133

Brammer, G. B., & van Dokkum, P. G. 2007, ApJ, 654, L107

Brammer, G. B., van Dokkum, P. G., & Coppi, P. 2008, ApJ, 686, 1503

Brinchmann, J., Charlot, S., White, S. D. M., Tremonti, C., Kauffmann, G., Heckman, T., & Brinkmann, J. 2004, MNRAS, 351, 1151

Bruzual, G., & Charlot, S. 2003, MNRAS, 344, 1000

Cameron, E., Carollo, C. M., Oesch, P. A., Bouwens, R. J., Illingworth, G. D., Trenti, M., Labbé, I., & Magee, D. 2010, arXiv:1007.2422

Daddi, E., et al. 2005, ApJ, 626, 680

de Vaucouleurs, G. H. 1959, Lowell Observatory Bulletin, 4, 105

Dickinson, M. 2000, Philosophical Transactions of the Royal Society of London, Series A, 358, 2001

Eyles, L. P., Bunker, A. J., Stanway, E. R., Lacy, M., Ellis, R. S., & Doherty, M. 2005, MNRAS, 364, 443

Förster Schreiber, N. M., et al. 2009, ApJ, 706, 1364

Franx, M., van Dokkum, P. G., Schreiber, N. M. F., Wuyts, S., Labbé, I., & Toft, S. 2008, ApJ, 688, 770

Genzel, R., et al. 2008, ApJ, 687, 59

Guo, Y., et al. 2009, MNRAS, 398, 1129

Hubble, E. P. 1926, ApJ, 64, 321

Kauffmann, G., et al. 2003, MNRAS, 341, 54

Kriek, M., van Dokkum, P. G., Franx, M., Illingworth, G. D., & Magee, D. K. 2009, ApJ, 705, L71

Labbé, I., et al. 2003a, AJ, 125, 1107

Labbé, I., et al. 2003b, ApJ, 591, L95

Lowenthal, J. D., et al. 1997, ApJ, 481, 673

Marchesini, D., et al. 2010, ApJ, 725, 1277

Mobasher, B., et al. 2005, ApJ, 635, 832

Oesch, P. A., et al. 2010, ApJ, 709, L16

Papovich, C., Dickinson, M., Giavalisco, M., Conselice, C. J., & Ferguson, H. C. 2005, ApJ, 631, 101

Peng, C. Y., Ho, L. C., Impey, C. D., & Rix, H.-W. 2002, AJ, 124, 266

Richard, J., Kneib, J.-P., Ebeling, H., Stark, D., Egami, E., & Fiedler, A. K. 2011, arXiv:1102.5092

Roberts, M. S., & Haynes, M. P. 1994, ARA&A, 32, 115

Salim, S., et al. 2007, ApJS, 173, 267

Sandage, A., & Tammann, G. A. 1981, Washington: Carnegie Institution, 1981, Preliminary version

Szomoru, D., et al. 2010, ApJ, 714, L244

Tacconi, L. J., et al. 2010, Nature, 463, 781

Toft, S., van Dokkum, P., Franx, M., Thompson, R. I., Illingworth, G. D., Bouwens, R. J., & Kriek, M. 2005, ApJ, 624, L9

Toft, S., et al. 2007, ApJ, 671, 285

Trujillo, I., et al. 2006, ApJ, 650, 18

van Dokkum, P. G., et al. 2008, ApJ, 677, L5

van Dokkum, P. G., et al. 2010, ApJ, 709, 1018

Wiklind, T., Dickinson, M., Ferguson, H. C., Giavalisco, M., Mobasher, V., Grogin, N. A., & Panagia, N. 2008, ApJ, 676, 781

Williams, R. J., Quadri, R. F., Franx, M., van Dokkum, P., Toft, S., Kriek, M., & Labbé, I. 2010, ApJ, 713, 738

Wuyts, S., Labbé, I., Schreiber, N. M. F., Franx, M., Rudnick, G., Brammer, G. B., & van Dokkum, P. G. 2008, ApJ, 682, 985

York, D. G., et al. 2000, AJ, 120, 1579